Carbon and hydrogen isotopic composition of methane over the last 1000 years

J. A. Mischler,[1] T. A. Sowers,[1] R. B. Alley,[1] M. Battle,[2] J. R. McConnell,[3] L. Mitchell,[4] T. Popp,[5] E. Sofen,[6] and M. K. Spencer[7]

Received 7 January 2009; revised 25 June 2009; accepted 4 August 2009; published 13 November 2009.

[1] New measurements of the carbon and hydrogen isotopic ratios of methane (δ^{13}C of CH_4 and δD of CH_4) over the last millennium are presented from the WAIS Divide, Antarctica, ice core (WDC05A), showing significant changes that likely were the result of human influences prior to the industrial revolution (at least as early as the 16th century of the common era (CE)). The δ^{13}C of CH_4 data corroborate the record from Law Dome, Antarctica, with high fidelity. The new δD of CH_4 data set covaries with the δ^{13}C of CH_4 record. Both δ^{13}C of CH_4 and δD of CH_4 were relatively stable and close to the present-day values from ~1000 to ~1500 CE. Both isotopic ratios decreased to minima around 1700 CE, remained low until the late 18th century, and then rose exponentially to present-day values. Our new δD of CH_4 data provide an additional independent constraint for evaluating possible CH_4 source histories. We searched a broad range of source scenarios using a simple box model to identify histories consistent with the constraints of the CH_4 concentration and isotope data from 990–1730 CE. Results typically show a decrease over time in the biomass-burning source (found in 85% of acceptable scenarios) and an increase in the agricultural source (found in 77% of acceptable scenarios), indicating preindustrial human influence on atmospheric methane as proposed in previous studies.

Citation: Mischler, J. A., T. A. Sowers, R. B. Alley, M. Battle, J. R. McConnell, L. Mitchell, T. Popp, E. Sofen, and M. K. Spencer (2009), Carbon and hydrogen isotopic composition of methane over the last 1000 years, *Global Biogeochem. Cycles*, *23*, GB4024, doi:10.1029/2009GB003460.

1. Introduction

[2] Ice cores provide high-resolution archives of the concentrations and isotopic ratios (δD and δ^{13}C) of atmospheric methane [*Sowers*, 2009; *Fischer et al.*, 2008; *MacFarling-Meure et al.*, 2006; *Sowers*, 2006; *Ferretti et al.*, 2005; *Sowers et al.*, 2005; *Etheridge et al.*, 1998]. CH_4 concentration measurements can be used to constrain estimates of CH_4 flux (involving sources and sinks of CH_4) over time while CH_4 isotope values provide additional information that is useful for resolving the relative importance of individual sources and sinks. Natural sources of CH_4 include wetlands, wildfires, termites, and ocean sediments, while rice paddies, ruminants, landfills, natural gas extraction, and biomass burning are the major anthropogenic sources (extensive review by *Reeburgh* [2004]). The isotopic composition of CH_4 from different sources has been measured over various temporal and spatial scales to estimate characteristic values of δD and δ^{13}C for each source. The $\delta^{13}CH_4$ and $\delta D(CH_4)$ data clearly distinguish isotopically enriched sources (e.g. biomass burning and natural gas venting) from depleted sources (e.g. wetlands and agricultural sources). Reconstructing atmospheric records of methane (both concentration and isotopic composition) from ice cores provides fundamental data to enhance our understanding of the global biogeochemistry of atmospheric CH_4.

[3] Because there are more distinct methane source types than isotopic tracers, and more spatially distributed sources than can be resolved by the geographically restricted suite of ice cores (only the ice cores of Antarctica and Greenland are known to provide reliable methane records), a unique inversion for the history of methane sources is not possible. However, the full suite of isotopic tracers and bipolar ice core data provides important boundary conditions for testing hypothetical methane source/sink histories, allowing elimination of large classes of scenarios.

[1]Department of Geosciences and Earth and Environmental Systems Institute, Pennsylvania State University, University Park, Pennsylvania, USA.
[2]Department of Physics and Astronomy, Bowdoin College, Brunswick, Maine, USA.
[3]Hydrologic Sciences Division, Desert Research Institute, Reno, Nevada, USA.
[4]Department of Geosciences, Oregon State University, Corvallis, Oregon, USA.
[5]Centre for Ice and Climate, Niels Bohr Institute, University of Copenhagen, Copenhagen, Denmark.
[6]Department of Atmospheric Sciences, University of Washington, Seattle, Washington, USA.
[7]Department of Geology and Physics, Lake Superior State University, Sault Saint Marie, Michigan, USA.

0886-6236/09/2009GB003460$12.00

1.1. Previous Work

[4] [*Ferretti et al.*, 2005] generated the first high-resolution $\delta^{13}CH_4$ record covering the last two millennia. Their record showed $\delta^{13}CH_4$ values that are very similar to present-day values between 0 and 1500 CE. After 1500 CE, their record exhibited an unexpected 2‰ decrease while the CH_4 concentration varied by less than 40 ppb (~2%). A broad $\delta^{13}CH_4$ minimum (−49‰) persisted for about one century before an increase to the present-day value (−47‰). This last $\delta^{13}CH_4$ change occurred during a period when the CH_4 loading of the atmosphere increased by over 100%, and is largely the result of additional anthropogenic sources that have enriched $\delta^{13}CH_4$ values. [*Ferretti et al.*, 2005] explained their results in terms of high baseline emissions of enriched CH_4 from biomass burning prior to 1500 CE. The decreasing $\delta^{13}CH_4$ values between 1500 and 1700 CE were ascribed to a decrease in biomass burning associated with a decline in the population of Central and South America following European contact.

[5] An alternate interpretation of the $\delta^{13}CH_4$ record was presented by [*Houweling et al.*, 2008], who attributed the heavy $\delta^{13}CH_4$ values prior to 1500 CE to elevated emissions of aerobic methane from plants (as discussed by *Keppler et al.* [2006]). *Houweling et al.* [2008] ascribed the drop in $\delta^{13}CH_4$ between 1500 and 1700 CE to the effects of an increase in the agricultural source (rice farming and animal husbandry) scaled to world population, in tandem with reduced plant growth and wetland emissions caused by the cooling of the Little Ice Age (LIA). *Houweling et al.* [2008] noted that this hypothesis requires the temperature change for the LIA to have been near the maximum published value [*Moberg et al.*, 2005], and that the temperature sensitivity for methane emissions needed to explain the $\delta^{13}CH_4$ drop was also close to the maximum published value.

[6] In this contribution we provide new records of $\delta^{13}CH_4$ and $\delta D(CH_4)$ covering the last 1000 years from the WAIS Divide ice core WDC05A. While we present data covering the entire 1000 year period, our discussion will focus only on the period between 990 and 1730 CE. We limit our discussion to this 740 year period in order to refine our understanding of the decoupling between the relatively constant atmospheric loading record and the unexpectedly large change in $\delta^{13}CH_4$. The abrupt exponential rise in CH_4 concentrations during the early 18th century prevents us from extending our analysis past 1730 CE. Model results using our new isotope records along with existing concentration records suggest changes in anthropogenic sources likely had a large impact on the atmospheric CH_4 budget during this period, which is consistent with the results of both [*Ferretti et al.*, 2005] and [*Houweling et al.*, 2008].

1.2. Chronology Development

[7] The WDC05A core (79°27.7′S 112°7.51′W; 1,759 masl) was drilled to 298.06 m during December of 2005. The drill site was located 1.3 km from the main WAIS Divide drill site, with a primary objective of reconstructing high-resolution atmospheric records covering the last 1,000 years. The upper 70 m of the core was processed for continuous ion chemistry [*McConnell et al.*, 2002], providing the most accurate means of constructing the ice age vs. depth model, with an absolute uncertainty of ±1 yr. In addition, continuous electrical conductivity and dielectric property (ECM/DEP) data were used to count annual layers over the entire core. The ECM/DEP records were independently counted by two individuals. The resulting age models agreed with one another within ±5%. The final ice age vs. depth model was constructed using the major ion data for the upper 70 m and the ECM/DEP counts between 70 m and 298 m.

[8] The age of the occluded gases is younger than the surrounding ice because air diffuses down through the firn more rapidly than snow is buried to the depth of bubble trapping in the firn/ice transition region (65–75 m below surface (mbs)). To estimate the ice age–gas age difference (Δage), a 1-D model of gas transport in the firn was developed for the site, following *Battle et al.* [1996] and *Trudinger et al.* [1997]. The transport model was used to estimate a mean gas age of 9.9 years at the top of the lock-in zone (65.5 mbs). The ice age at this level was 215 years at the time of coring, making Δage equal to 205 years. Annual layer thickness data from the ECM/DEP counts suggest the accumulation rate at our site has remained constant over the last 1,000 years. Isotope temperature records from the core are not yet available to infer a surface temperature record. We therefore assume that Δage values have remained constant throughout the record. The gas age vs depth model for the WDC05A core was established by subtracting 205 years from the ice age at every dated depth below 65.5 mbs. We estimate the uncertainty associated with the mean gas age assignment as ±5%, but note that comparison of the detailed CH_4 record from WDC05A with the Law Dome CH_4 record from *MacFarling-Meure et al.* [2006] suggests our gas age model is probably good to within a decade relative to the Law Dome chronology (L. Mitchell et al., manuscript in preparation, 2009).

2. Analytical Methods

[9] Firn air was collected according to the methods of *Battle et al.* [1996] and analyzed directly from flasks for $\delta D(CH_4)$ and $\delta^{13}CH_4$ as by *Sowers et al.* [2005]. The "wet" extraction procedures used in this study for liberating relict air from ice samples followed by mass spectrometric determination of the $\delta D(CH_4)$ and $\delta^{13}CH_4$ were similar to those described by *Sowers* [2006] and *Sowers et al.* [2005], respectively. Ice samples between 1–1.6 kg for δD (0.4–0.7 kg for δ^{13}C) were cut from larger core sections in order to obtain sufficient amounts of trapped CH_4 for $\delta D(CH_4)$ and $\delta^{13}CH_4$ analysis. Between the base of the firn-ice transition (75 mbs) and the bottom of the core (298.06 mbs) a total of 58 samples were analyzed for $\delta^{13}CH_4$ and 40 samples for $\delta D(CH_4)$. This sampling strategy yielded records that have a resolution of 20 years for both δD and $\delta^{13}CH_4$ from the 15th century to around the 1970s (although there is a notable gap in the $\delta^{13}CH_4$ data from the late 16th century through the late 17th century), with lower resolution sampling for both records stretching back to 1160 CE (and into the first millennium CE for $\delta^{13}CH_4$). The $\delta D(CH_4)$ record contains small gaps in the data set centered around the late 1790s and the 1930s, while minor gaps are apparent in the $\delta^{13}CH_4$ data

Table 1. Verification of Analytical Method

System Tested	Method	N	$\delta^{13}C$(‰)	Std Dev	Meas. − Accept.[a]
Analytical	Flask[b]	100	−46.9	0.1	0.2
Extraction	BFI[c]	16	−47.4	0.2	−0.3
System Tested	Method	N	δD(‰)	Std Dev	Meas. − Accept.[a]
Analytical	Flask[b]	46	−86	3	−2
Extraction	BFI[c]	5	−85	2	−1

[a]Accepted value provided by Stan Tyler (UCI), CH_4 concentration = 1776 ppb, $\delta^{13}C$ = −47.16‰, δD = −84.3‰.

[b]Standard equilibrated into glass flasks and put directly into the analytical system.

[c]Standard equilibrated over bubble free ice (BFI) and ran through both the extraction system and the analytical system.

in the late 18th century and late 19th century. A uniformly sampled data set was not achieved because: 1) some areas did not have sufficient good quality ice; and/or 2), problems were encountered during the extraction/analytical procedure and the data had to be rejected.

2.1. Sample Processing and Analysis

[10] The outer ∼5 mm of each core section was shaved away using a band saw to expose fresh ice core. Each shaved ice sample was sealed into a stainless steel (SS) cylinder using a copper gasket, and evacuated for 1 hour to remove the ambient air from the sample cylinder and sublimate a thin film of ice from the sample. The evacuated cylinder was then isolated and placed within a ∼ 40°C warm water bath (45 min for δD, 30 min for $\delta^{13}C$) to completely melt the ice sample and release the trapped sample air into the headspace of the cylinder above the meltwater. The cylinder was then placed into a large SS Dewar where the meltwater was refrozen using liquid nitrogen. After the meltwater was completely frozen (45 min for δD, 30 min for $\delta^{13}C$), the sample cylinder was connected to the evacuated extraction line. The cylinder headspace was flushed with ultra-high-purity (UHP) He (40 cc/min) until the sample air was quantitatively (∼95%) removed from the cylinder (one hour for δD, 45 min for $\delta^{13}C$). The sample air was passed through a water trap (−110°C) and a methane trap (HaySep D at −130°C) where CH_4 in the sample air was adsorbed onto the HaySep D material. The methane trap was then isolated, removed from the extraction system, and attached to a PreCon peripheral device for CH_4 isotopic analysis following *Sowers et al.* [2005] and *Sowers* [2006].

2.2. Method Verification, Corrections, and Uncertainties

[11] An independent house standard (CA 04826) ($\delta^{13}C_{assigned}$ = −47.13 ± 0.01‰, $\delta D_{assigned}$ = −84.3 ± 1.6‰) was used to establish the integrity of the extraction process at various times during the period when we extracted the ice samples (Table 1). This high-pressure air cylinder was filled during a research cruise in the South Pacific [*Rice et al.*, 2001], and assigned CH_4 isotope values based on analyses by Stan Tyler at the University of California, Irvine. The extraction system was tested by expanding an aliquot of the house standard (CA 04826) over bubble-free ice (BFI) produced in the lab, then sealed in a cylinder and processed in the same manner as the samples. The BFI was run through a freeze/thaw cycle, and the resulting headspace gas was flushed through the extraction system as described previously. This process was repeated 16 times for $\delta^{13}CH_4$ (mean value = −47.4 ± 0.2‰, −0.3‰ from the assigned value) and five times for $\delta D(CH_4)$ (mean value = −85 ± 2‰, −1‰ from the assigned value) (Table 1). The difference between the assigned standard value and the measured value during simulated sample runs may arise in part because when the ice sample is melted some of the trapped methane is absorbed into the meltwater according to Henry's Law. When the sample is then refrozen a small amount of the CH_4 is trapped in the ice matrix. Estimates of the isotopic composition of CH_4 in equilibrium with water suggest the $\delta^{13}CH_4$ of CH_4 in the meltwater should be 0.3‰ higher than the headspace gas [*Knox et al.*, 1992]. Based on our estimate of how much of the total amount of CH_4 present in the sample we were able to extract (∼95%) and the partition of CH_4 between the headspace and water in the vessel, we calculate that this effect may have raised the $\delta^{13}CH_4$ in our samples by less than 0.1‰, not enough to account for the enriched nature of the simulated transfers. The remainder of the offset between the assigned value and the simulated transfer results must be the result of very small isotope fractionation processes associated with our technique. We have corrected our data set for this offset.

[12] All uncertainties for the data points were assessed based on the uncertainties measured for the simulated trapped-gas extractions, in which the standards were processed in exactly the same way as our samples, including the mass spectrometric analyses and their corresponding corrections. We believe this is the most representative means of conveying the true analytical uncertainty, yielding ±0.2‰ and ±3‰ for $\delta^{13}CH_4$ and $\delta D(CH_4)$, respectively. The analytical system was tested by equilibrating the house standard CA 04826 into glass flasks (50−200 cc) and directly analyzing these standard flasks at the beginning of each day before sample runs. If the daily standard runs differed too much (more than 0.2‰ for $\delta^{13}C$ and 3‰ for δD) from the mean value of the average of recent previous runs, additional standards were run until a stable isotope value for the standard was obtained.

[13] These standard measurements (100 for $\delta^{13}C$ and 36 for δD) resulted in mean values for the standard CA 04826 flask samples on our system (−46.9 ± 0.1‰ for $\delta^{13}C$ and −86 ± 3‰ for δD) that were offset (∼0.2‰ for $\delta^{13}C$ and ∼−2‰ for δD) from the values determined by Tyler (Table 1). Great efforts have been made to minimize the offset between the daily measurements and the assigned values. We believe the offset stems from long-term drift in the oxidation/thermal conversion furnaces, which are difficult to control on a day-to-day basis. To account for these day-to-day furnace fluctuations, we have chosen to correct all samples run on a particular day for the difference between the measured standard value and the assigned value. The magnitude of this correction is generally less than 0.2‰ and 3‰ for $\delta^{13}C$ and δD, respectively. This correction assumes the offset is nearly constant throughout a day of measurements, which we have verified by running multiple standards during some days.

[14] Additionally, the δD data must be corrected for what is termed the "viscous flow effect". In our D/H analytical technique, H_2 reference peaks (Oztech Corp.) for each run were introduced into the mass spectrometer source from the bellows as opposed to the gas bench where the sample comes in. An experiment was performed to determine the zero enrichment of this system by placing an aliquot of UHP (5.0) H_2 from a large tank feeding the Gas Bench into the bellows of the mass spectrometer and running it against the original tank via the Gas Bench. The resulting zero enrichment showed substantial offset that scaled with the pressure in the bellows (higher offset at lower bellows pressure). We surmise that the offset arises at the capillary crimp where the pure H_2 from the bellows passes into a He background in the source. A viscous flow correction curve was generated every week with a range of standard pressures corresponding to those extant during a normal run. Individual samples were corrected based on the standard peak intensity for that run. Normally the viscous flow correction ranges between -4.5‰ and -5.5‰ and was applied to samples and standards. Finally, a correction for H_3 production in the source was made following *Sessions et al.* [2001].

[15] Both the $\delta D(CH_4)$ and $\delta^{13}CH_4$ data sets were corrected for gravitational effects (-0.31‰) according to *Sowers et al.* [1989]. Gravitational fractionation in the firn is mass-dependent, such that the heavier isotopologues of CH_4 are preferentially concentrated at the base of the firn. The $\delta^{15}N$ of N_2 of the atmosphere is essentially constant over millions of years and also influenced by gravitational fractionation [*Sowers et al.*, 1989]. We use the measured $\delta^{15}N$ of N_2 at the base of the firn (+0.31‰, J. Severinghaus, personal communication, 2008) to correct all our CH_4 isotope data for gravitational fractionation.

[16] Both the $\delta D(CH_4)$ and $\delta^{13}CH_4$ data sets were also corrected for diffusional effects that arise from atmospheric concentration changes. As the concentration of an atmospheric constituent varies, the surface values are propagated down into the firn by diffusion. Because the diffusivity of a $^{13}CH_4$ (or a $^{12}CH_3D$) molecule is 1.8% lower than that for the $^{12}CH_4$ species [*Trudinger et al.*, 1997], increasing atmospheric CH_4 produces a drop in both the firn air $\delta^{13}CH_4$ and $\delta D(CH_4)$ relative to the overlying atmospheric value. To correct our measured values for this effect, we utilized the 1-D firn-air transport model of *Battle et al.* [1996] and the Law Dome CH_4 record to estimate the magnitude of the diffusion correction. The correction is largest during periods when CH_4 increases most rapidly. The largest corrections ($\sim$1.2‰) were required for the data from just below the firn/ice transition region (75–85 m).

3. Analytical Results

[17] The $\delta D(CH_4)$ and $\delta^{13}CH_4$ trends over the last 1000 years are shown in Figure 1 along with the CH_4 concentration curve generated by *MacFarling-Meure et al.* [2006]. The $\delta^{13}CH_4$ data generated by *Ferretti et al.* [2005] are also displayed for comparison. There is remarkable agreement between the two $\delta^{13}CH_4$ data sets, considering they were generated from different cores with different timescales and in separate labs. This indicates that these data sets are reliable and record the past levels of $\delta^{13}CH_4$ with high fidelity. We present the first $\delta D(CH_4)$ record for this period, and note that the shape of this record is very similar to the $\delta^{13}CH_4$ record. As shown in Figure 1, both the $\delta D(CH_4)$ and $\delta^{13}CH_4$ started to decrease at $\sim$1460 CE, which is also when CH_4 began an abrupt $\sim$30 ppb rise. Both $\delta D(CH_4)$ and $\delta^{13}CH_4$ continued to decrease as CH_4 reversed its trend and suddenly decreased (average drop of $\sim$20 ppb) starting in the 1580s CE. CH_4 remained low while $\delta D(CH_4)$ and $\delta^{13}CH_4$ reached their lowest values until all three increased from the late 18th century onward. As mentioned previously, the focus of this work is the 740 year period that ends in the middle of the 18th century. We have also measured ice core and firn air samples that extend these records to the present day and are included in Figure 1. These $\delta D(CH_4)$ data show a trend similar to that of $\delta^{13}CH_4$, which one expects given that most industrial CH_4 sources are enriched in both heavy isotopes. We have chosen to present these data to illustrate the abrupt isotope changes that have occurred during the last century. However, as the focus of the present contribution extends only to the 18th century, we do not discuss the significance of the latest isotope results in terms of specific industrial sources.

[18] All of our data are shown in Figure 1, but the five data points (three $\delta^{13}CH_4$ and two $\delta D(CH_4)$) plotted with star symbols are considered "outliers" and are not included in subsequent analyses. Outliers were flagged in the laboratory if sampling conditions or protocols fell outside of our accepted procedures (e.g., extraction errors). In addition, even if no errors were detected in sample processing, a point was identified as an outlier if it differed from the mean of its nearest neighbors, calculated from the two samples (one immediately preceding and one immediately following), by more than twice the standard deviation of those neighboring samples. Also, analyses of firn air and ice within 5m of the bubble close-off region (70–75 m) appear to be compromised by partial extraction of recently closed bubbles that yield "light" isotope values. Data from this interval are also identified as outliers using the star symbols in Figure 1.

4. Modeling Methods

[19] The following sections describe our use of a box model of atmospheric methane to invert for changes in source strengths consistent with the reconstructed changes in methane concentration and isotopic ratios. The atmospheric methane model used in this study has been modified from that of *Tans* [1997]. It consists of two perfectly mixed boxes, corresponding to the Northern and Southern hemispheres, with an interhemispheric exchange time fixed at 1 year. The lifetime of methane (which governs the rate of methane destruction) was also held constant at 7.6 years for both hemispheres, consistent with previous work [*Houweling et al.*, 2000b; *Lassey et al.*, 2000; *Ferretti et al.*, 2005]. The model allows independent methane sources in the Northern and Southern hemispheres, and a single methane sink acting on both boxes. Each model run was allowed to reach steady state for the given input parameters.

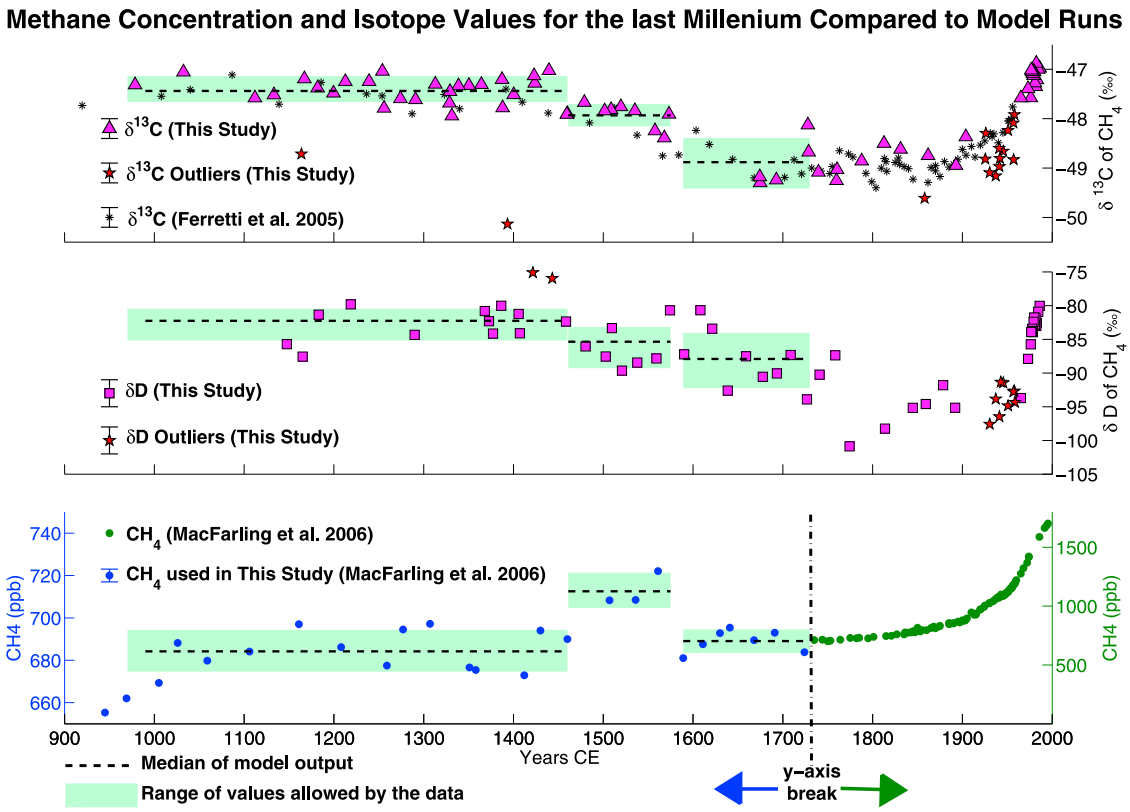

Figure 1. The $\delta^{13}CH_4$, $\delta D(CH_4)$ and CH_4 concentration data referred to in this study for time slice 1 (TS1) (990–1460 CE), TS2 (1461–1575 CE), and TS3 (1589–1730 CE). Analytical uncertainties are indicated with ±1 standard deviation about the symbol in the figure legends. (top) The $\delta^{13}CH_4$ data from *Ferretti et al.* [2005] are plotted along with the $\delta^{13}CH_4$ data from WDC05A including results from firn air analyses covering the period 1950 CE to present. Outlying data are presented with stars as discussed in the text. (middle) The $\delta D(CH_4)$ data from WDC05A on the SMOW isotope scale including results from firn air analyses covering the period 1950 CE to present. Outlying data are presented with stars as discussed in section 3. (bottom) The CH_4 data from *MacFarling-Meure et al.* [2006] (note the y axis scale change at 1730 CE). Shaded regions correspond to ±1 standard deviation about the mean of all data per time slice (TS). These shaded regions denote the range of acceptable data values for each data set per TS and are used to constrain the model output. Note that the time scales for the isotope data have been shifted forward by 20 years to account for the time lag for the atmospheric CH_4 isotopic values to reach equilibrium relative to CH_4 concentration changes [*Tans*, 1997]. Dashed horizontal lines through each TS shaded region denote the median values for each data series based on the primary model results.

[20] In reality there is a diverse set of methane sources and sinks, which are distributed nonuniformly across the Earth's surface. In light of the underconstrained nature of the problem, we follow previous workers by consolidating the large range of sources and sinks into a smaller number of categories. The CH_4 sources were divided into four categories: agricultural, geologic, natural microbial ($natural_{Mic}$), and biomass burning. Each category was assigned a unique isotopic value for both the $\delta D(CH_4)$ and $\delta^{13}CH_4$ (Table 2), and these values were held constant while the magnitude of each category's emissions was allowed to vary from one run to the next within a range provided by the literature (references found in Table 2). In this way we used the model to generate all possible source strength scenarios for the emission ranges shown in Table 2. The sinks were likewise consolidated into one sink term with characteristic fractionation factors for $\delta^{13}C$ and δD. The fractionation factors and relative contributions for the major sinks of methane (as described in section 4.2 and Table 3) were held constant throughout the model runs. We believe that these ranges encompass all possible combinations of emissions.

4.1. Source Characterization

[21] All source category isotopic values and emission ranges (as well as their associated references) are described in detail in Table 2. The high and low ends of the source strength ranges for each emission category were determined using the highest and lowest estimates found in the literature (references found in Table 2), in order to consider the widest range of possibilities. We believe that these ranges are somewhat broader than needed to capture actual emissions, and thus that we have successfully searched the likely combinations of emissions.

Table 2. Source Parameters Used for Model Runs

Source	Emission Range (Tg/yr (10^{12} g/yr))	Step (Tg/yr)	$\delta^{13}C$[a] (‰)	δD[a] (‰)	NH[b] (%)	SH[b] (%)
Agricultural	0 to 60[c]	1	$-63^{d} \pm 5^{d}$	$-330^{d} \pm 15^{d}$	80	20
Geologic	5[e] to 53[f]	1	-38 ± 7^{g}	-175 ± 20^{g}	90	10
Natural$_{Mic}$	92[h] to 232[h]	1	$-57^{i} \pm 5^{g}$	-322 ± 20^{g}	77	23
Biomass burning	5[e] to 45[j]	1	$-23.6^{k} \pm 2^{k}$	$-169^{k} \pm 21^{k}$	44	56

[a]Mean isotope values were used in the model; ranges are shown only to indicate the uncertainty in each value from the literature. Isotope values are from *Tyler et al.* [2007] unless otherwise stated.
[b]Hemispheric distribution of sources taken from *Marik* [1998].
[c]On the basis of the maximum value suggested by *Ruddiman and Thomson* [2001] at 1700 CE.
[d]The mean isotopic values and standard deviation for the agricultural source were determined by weighting the isotopic values of rice cultivation and animal husbandry by the emission values from *Lassey et al.* [2007]. The isotopic value for rice was determined using the studies of *Uzaki et al.* [1991], *Levin et al.* [1993], *Tyler et al.* [1994], *Bergamaschi* [1997], *Chanton et al.* [1997], *Kruger et al.* [2002], *Nakagawa et al.* [2002], and *Han et al.* [2005], and the isotopic value for CH_4 released from the rumen of farm animals was determined using the studies of *Rust* [1981] and *Levin et al.* [1993].
[e]Taken from mean value for preindustrial emissions given by *Lassey et al.* [2007].
[f]Maximum value taken as the mean from *Etiope et al.* [2008].
[g]Uncertainties taken from *Quay et al.* [1999].
[h]Emission Range taken from *Wuebbles and Hayhoe* [2002], and references therein.
[i]Weighted average of all natural microbial sources (termites, tundra, lakes, swamps, and marshes) with relative contributions and isotope values taken from the budget of *Tyler et al.* [2007], and references therein.
[j]Mean value suggested from model runs by *Fischer et al.* [2008].
[k]Mean global value and uncertainties calculated from *Yamada et al.* [2006].

[22] The agricultural source category contains contributions from both rice cultivation and animal husbandry. The relative contribution of each was determined using a weighted average calculated from the separate 1700 CE emission rates given in [*Lassey et al.*, 2007], which are assumed to hold for all "low-emission" time intervals before the onset of rapid global population growth in the 1730s. Rumen studies involving diets high in corn were omitted because corn was not commonly used as livestock feed during the preindustrial era [*Turner et al.*, 2001]. The isotopic value for rice was determined by averaging the mean isotopic values from a number of rice studies conducted in both humid tropical and humid subtropical regions (Table 2). Numerous natural sources of microbially produced CH_4 (termites, tundra, lakes, swamps, and marshes) are included in the natural$_{Mic}$ source category (Table 2). The geologic source includes natural hydrocarbon seepage and venting, whereas the contribution of CH_4 from anthropogenic burning of fossil fuels before 1730 CE was taken to be negligible following *Andres et al.* [1999]. All isotopic values chosen for these model runs are consistent with previous studies within the uncertainty range introduced by heterogeneity of values within each source class [*Levin et al.*, 1993; *Khalil*, 1993; *Quay et al.*, 1999; *Houweling et al.*, 2000a; *Lassey et al.*, 2000; *Tyler et al.*, 2007].

[23] It is clear from Table 2 that there is much less of a distinction between the isotopic values of the agricultural and natural$_{Mic}$ sources than any other pair of sources listed. Due to their similarity, it is likely that in some cases a change in one of these two sources is partially compensated by an opposing change in the other source. This phenomenon is fully captured in our modeling approach, which tests all possible combinations. If the agricultural and natural$_{Mic}$ sources were more distinct in their isotopic values, the suite of possible source strengths for each time period would be more tightly constrained.

4.2. Sink Characterization

[24] This model incorporates a single sink term with corresponding kinetic isotope effects for both the $\delta^{13}CH_4$ and $\delta D(CH_4)$ (KIE_{13C} and KIE_D respectively). In order to determine these KIEs, three key sinks of methane were identified (oxidation by tropospheric species [OH], oxidation by stratospheric species [OH, Cl and $O(^1D)$], and oxidation in soils). Another possible sink term, here called the marine boundary layer chlorine sink, has been suggested by the modeling work of *Allan et al.* [2007]. To date there

Table 3. Sink Kinetic Isotope Effect (α) Values Used in Model Runs[a]

Sink	Relative Contribution[b] (%)	α_{13C} $k(^{13}CH_4)/k(^{12}CH_4)$	ϵ_{13C}[c] ‰	α_D $k(^{12}CH_3D)/k(^{12}CH_4)$	ϵ_D[c] ‰
Troposphere	88 ± 2.9	0.9961 ± 0.0004^{d}	(-3.88 ± 0.4)	0.7729 ± 0.0108^{d}	(-227 ± 11)
Stratosphere	7 ± 2.6	0.9847 ± 0.0047^{e}	(-15.3 ± 4.7)	0.7005 ± 0.0294^{f}	(-299 ± 29)
Soils	5 ± 3.4	0.9824 ± 0.0032^{g}	(-17.6 ± 3.2)	0.8764 ± 0.0795^{g}	(-124 ± 79)
Total[h]	—	0.9946 ± 0.0008	(-5.40 ± 0.84)	0.7731 ± 0.0155	(-227 ± 16)

[a]Shown with ϵ (‰) equivalents.
[b]Relative contributions from each sink determined by the sink strengths found in the work of *Reeburgh* [2004], and references therein.
[c]The ϵ value for each sink was calculated via the relationship: $\epsilon = 1000(\alpha - 1)$.
[d]*Saueressig et al.* [2001].
[e]Mean value for range given by *Rice et al.* [2003].
[f]*Rhee et al.* [2006].
[g]Average of mean values found in the work of *Mahieu et al.* [2006], and references therein.
[h]The total CH_4 sink magnitude was parameterized via the lifetime of CH_4 (held constant at 7.6 years for all model runs).

have been no studies confirming the existence of this sink by actual Cl radical measurements, and its magnitude and long-term temporal variation are not well constrained. Therefore, we follow *Fischer et al.* [2008] by not including this sink in our composite sink term, although we do explore how changes in the composite sink term affect the median source strengths in our sensitivity runs (discussed in section 4.5). All values used in determining the single sink term are shown in Table 3.

4.3. Modeling Approach

[25] Our approach centers on using the CH_4 concentration and isotope data in Figure 1 as target values for assessing the relative contribution of various sources with fixed characteristic isotope values. A fully time-dependent inversion for source strengths would be sufficiently underconstrained that we do not attempt it. Instead, we have identified three time slices (TS1, TS2, TS3) that are sufficiently long and during which CH_4 concentrations are reasonably stable. Then, to avoid short term variations in the data from interfering with detection of longer term (multidecadal) trends, we simply averaged each of the three data sets (CH_4 concentrations, $\delta^{13}CH_4$, and $\delta D(CH_4)$) over each time slice to obtain representative values for each data set for each time slice.

[26] During the first time slice (TS1, 990–1460 CE), CH_4 averaged 684.0 ppb. During the second time slice (TS2, 1461–1575 CE), the average CH_4 concentration was higher, at 713.8 ppb. The average methane concentration during the third time slice (TS3, 1589–1730 CE) was 689.5 ppb, similar to the average during TS1; the exponential increase in CH_4 during the industrial era began after TS3. Because the isotopic composition of atmospheric CH_4 requires a few decades to approach steady state following a perturbation [*Tans*, 1997], all isotopic data are reported after subtracting 20 years from their CE date, such that isotopic ratios of gas samples yielding ages of 1010–1480 CE are plotted in Figure 1 as having ages 990–1460 CE, and similarly for the other time slices.

[27] For each time slice, we use the model to determine those combinations of source strengths that are consistent with the mean CH_4 concentration, $\delta^{13}CH_4$ and $\delta D(CH_4)$ in each time slice, and with the independent constraints provided by the literature and detailed in Table 2. For our primary runs, all isotopic values were held fixed, and all combinations of source strengths were tested within the ranges defined by Table 2. A second set of runs duplicated these primary runs, but with the additional constraint that the agricultural CH_4 sources varied directly with population, to test whether such additional information would notably reduce uncertainties in estimates of other source strengths. Finally, a set of sensitivity runs was completed to evaluate the effect of individual small changes in source isotopic ratios and in sink fractionation factors to provide the reader some guidance on the effect of such changes on estimated methane source strengths. Additional improvements in knowledge of the allowable range of isotopic ratios of individual sources, and in modeling, may in the future justify the now impractical effort of searching through all allowable source strengths and isotopic ratios for optimal solutions.

4.3.1. Primary Run

[28] For each of the four sources, we stepped from the minimum to the maximum source strength as listed in Table 2, in increments of 1 Tg/year; we conducted model runs to steady state for every possible combination of these sources, for a total of 17,279,409 forward model runs. The partitioning of each source into Northern and Southern Hemisphere boxes (partitioning shown in Table 2) was maintained the same in all runs, as were all other parameters except for the source strengths. Each model run produced a steady-state methane concentration, $\delta^{13}CH_4$ and $\delta D(CH_4)$ for each hemisphere. The output of each run was evaluated for consistency with the observed data (CH_4 concentration, δD and $\delta^{13}CH_4$ in the southern box, which encompasses our data sources) for each of the three time slices. A result was considered to be consistent with the data if it matched all three of the constraints (concentration and both isotopic ratios) within the uncertainty in the data, which was taken as one standard deviation from the average for each constraint for each time slice. In light of our experience with the entire process of data collection and interpretation, we decided that in this particular case it is more appropriate to use the standard deviation rather than the more conventional standard error to construct these ranges of allowable values (though we have chosen half of the conventional ±2 standard deviations) (Figure 1, horizontal boxes). For most of the data, the standard error is smaller than the actual analytical uncertainty associated with measurement of $\delta^{13}CH_4$ and $\delta D(CH_4)$. Because the actual analytical uncertainty may involve systematic as well as random errors, we did not consider it appropriate to use the standard error.

[29] All runs that matched the CH_4, $\delta D(CH_4)$, and $\delta^{13}CH_4$ constraints for a time period were saved. The 12,224 acceptable runs for the first time slice (TS1) (and independently, the 18,562 for the second time slice (TS2) and 57,672 for the third slice (TS3)) are displayed in a box-and-whisker plot (Figure 2, boxes to the left). The boxes in Figure 2 encompass the middle 50% of the model results that best characterized the data, and the "whiskers" are drawn to encompass all outlying data points.

[30] To illustrate the utility of using $\delta D(CH_4)$ as an additional constraint, the results of the primary run (including $\delta D(CH_4)$ data) were compared to those in which $\delta D(CH_4)$ data were not used. For every time slice and source category considered, the allowable source strengths were more tightly constrained when including the $\delta D(CH_4)$ constraint. In the most extreme case the total range of source strengths (the whiskers) for the geologic source in TS1 was reduced by 58% while the box width was reduced by 75%.

[31] To test whether our chosen hemispheric distribution of sources and sinks produces acceptable results, we compared the observed and modeled interhemispheric gradients in CH_4. The data [*Etheridge et al.*, 1998] are sufficient to allow this test during TS1. The model gradient for the medians of the acceptable TS1 source strengths is 40 ppb, versus 43 ± 20 ppb measured. Because the data sources are towards the poles but the box model averages each hemisphere from pole to equator, the model should slightly underestimate the observed value. The general agreement of data and model shows that our chosen hemispheric

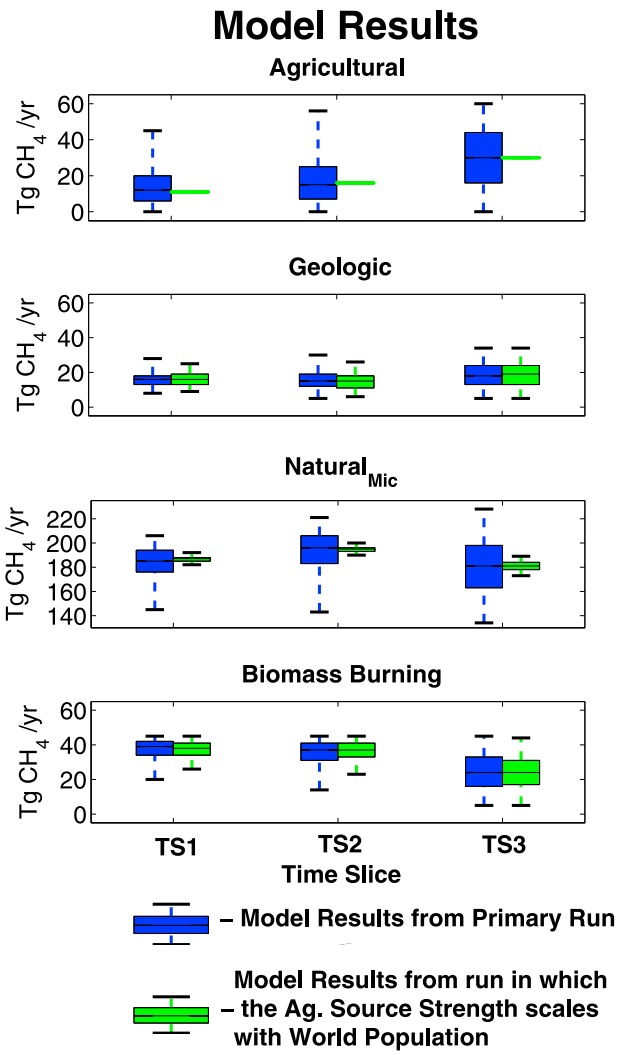

Figure 2. Box plot of model results for TS1 (990–1460 CE), TS2 (1461–1575 CE), and TS3 (1589–1730 CE). Acceptable model runs are shown for both the primary run (darker box shown on the left in each case) and the run in which the agricultural source scales with population (lighter box to the right), for all three time slices and for all four source categories. Following convention, the box in each case includes 50% of the acceptable runs, and the "whiskers" include all acceptable runs. Note that the trends between time slices are similar supporting the coupling between population and CH_4 emissions. Scaling the agricultural source to population narrows the acceptable ranges without notably changing the medians.

distribution of sources and sinks is consistent with this constraint. However, given the limitations of the data, and of the two-box model versus the point data from Greenland and Antarctica, we do not believe that it is warranted to use the observed interhemispheric gradient to adjust the observed hemispheric distribution of sources and sinks.

[32] To assess whether the strength of a particular methane source category changed significantly (with >95% confidence) within a given model run type (i.e., the primary run, the runs in which the agricultural source scaled with population, and the sensitivity runs), we followed *Ott and Longnecker* [2001] in calculating the two-way Wilcoxon rank sum test for the difference between the medians of the acceptable model output for TS1 compared to TS3. We chose to compare TS1 to TS3 in order to investigate the maximum difference in isotopic values between time slices. The Wilcoxon rank sum test indicates (by virtue of the very tightly constrained confidence intervals around the median values) that all changes in the median values observed within runs (from TS1 to TS3), for all model run types, are significant.

[33] However, these tests regarding the median clearly do not capture the full distributions of the model-run outputs. In our formulation, each of the accepted source strengths in the model output for a given time slice is equally likely to be correct, so randomly choosing one value for a given source from TS1 and one value from TS3 defines a possible history. To assess the tendency for increase, no change, or decrease within a model run type, we randomly selected 10% of the accepted model outputs for each source category for TS1 and TS3, and formed all combinations of this subset for each source category. This process was repeated for each model run type (we call this the "sign test"). We report our results for each source category within each run type as the percent of: 1) runs for which the particular source category increased from TS1 to TS3, 2) runs for which the particular source category did not change from TS1 to TS3 and, 3) runs for which the particular source category decreased from TS1 to TS3. The sign test results for the primary run and the run for which the agricultural source was made to scale with population are tabulated in Table 4.

4.3.2. Test With the Agricultural Source Scaling With World Population

[34] It has been proposed that agriculture, and presumably the agricultural methane source, has increased with world population over time [*Pongratz et al.*, 2008; *Houweling et al.*, 2008] (though *Ruddiman and Thomson* [2001] assert that agricultural CH_4 emissions need not have been coupled with population over the last few thousand years). If methane emissions were coupled with world population over the last millennium, then this provides a way to more tightly constrain estimates of changes in other sources over time. As a means of exploring this relationship, the three median values for agricultural source emissions (one from each time slice) were taken from the primary run values as shown in Figure 2, and each was plotted versus the corresponding average world population from *McEvedy and Jones* [1978]. An exponential curve (R^2 = 0.98) fit these three data points better than a linear regression (R^2 = 0.94) and therefore was chosen to represent the relationship between the agricultural source and world population. The three agricultural source emission values were then adjusted (none by more than 1 Tg/yr) so that they fell directly on the curve. Three separate sets of model runs (one for each time slice), each using one of these "new" agricultural values (while all other emission ranges were varied across their full ranges, as previously stated), were then initiated. The runs for which data and model were in agreement were collected as before, and the significance and sign of each change was

Table 4. Comparison of Results from the Primary Run and the Run for Which the Agricultural Source Scales With World Population

	Median Source Values				Percent of Scenarios Where...					
	TS1[a](Tg/yr)		TS3[b](Tg/yr)		TS1 < TS3[c]		TS1 = TS3[d]		TS1 > TS3[e]	
Source	Prim[f]	Ag[g]	Prim[f]	Ag[g]	Prim[f]	Ag[g]	Prim[f]	Ag[g]	Prim[f]	Ag[g]
Agricultural	12	11	30	30	77	NA	2	NA	21	NA
Geologic	16	16	18	19	59	63	5	4	37	33
Natural$_{Mic}$	185	187	181	181	44	15	1	6	54	79
Biomass burning	39	38	24	24	13	10	2	2	85	88

[a]TS1 (Time Slice 1) spans 990 to 1460 CE.
[b]TS3 (Time Slice 3) spans 1589 to 1730 CE.
[c]Indicates percentage of scenarios for which the designated source increased from TS1 to TS3.
[d]Indicates percentage of scenarios for which the designated source remained constant from TS1 to TS3.
[e]Indicates percentage of scenarios for which the designated source decreased from TS1 to TS3.
[f]Results obtained from the Primary Run (Prim) in which all source categories were allowed to range between their respective maximum and minimum values as shown in Table 2.
[g]Results obtained from the run in which the agricultural source was made to scale with world population (Ag) and all other source categories were allowed to range as in the Primary Run.

determined as done previously (Table 4). These results are plotted with the primary run on Figure 2 (boxes to the right).

4.3.3. Model Sensitivity to Isotopic Variation

[35] In all of the model runs described above, each of the four methane sources was assigned a unique $\delta^{13}CH_4$ value and $\delta D(CH_4)$ value (shown in Table 2) and each of the sinks was associated with a unique KIE (Table 3), and these were held constant throughout all of the model runs. Separate sensitivity model runs were conducted to explore the effect of slight variations in these isotopic values within their uncertainties. Variations of either $-1‰$ $\delta^{13}CH_4$ or $-5‰$ $\delta D(CH_4)$ were individually applied to each source and the total sink term (+0.001 and +0.005 change to the α_{13C} and α_D respectively) in order to estimate the effect on each of the median values of the resulting source strengths. This set of ten runs (separate shifts in carbon and in hydrogen for four source types and for the sink) was then analyzed as before, without constraining the agricultural source to follow population. The results were compared as before using the two-way Wilcoxon rank sum test and sign test to learn whether the changes in the source medians from TS1 to TS3 that were significant in the primary runs were still significant in the sensitivity runs. The results of the sensitivity runs were also compared to the results from the primary run, using the sign test and the one-way Wilcoxon test, in order to: 1) compare the sensitivity run data sets to the medians of the 4 source categories in the primary run, to see if the medians of the 4 source categories changed significantly from the primary run to the sensitivity runs and, 2) determine what effect these changes in isotopic values of the source/sink terms have on the magnitudes of the source strength medians. None of the data sets generated in the sensitivity runs had medians that were significantly different from the corresponding medians found in the primary runs.

5. Modeling Results

5.1. Model Results for the Primary Run

[36] As shown in Figure 2, the median values of the four source strengths exhibit trends across the three time slices examined. From the first time slice (TS1) to the third time slice (TS3) there is strong evidence for an increase in the agricultural source (77% of scenarios indicate an increase from TS1 to TS3, 2% no change, 21% decrease, median change of 18 Tg/yr) (Table 4) while there is comparatively little evidence for a directional change in the geologic source (59% increase, 5% no change, 37% decrease, median change of 2 Tg/yr) or a change in the natural$_{Mic}$ source (44% increase, 1% no change, 54% decrease, median change of -4 Tg/yr). There is strong evidence for a drop in biomass burning from TS1 to TS3 (13% increase, 2% no change, 85% decrease, median change of -15 Tg/yr) (Table 4).

5.2. Model Results for the Agricultural Source Scaling With Population

[37] The trends over time in the methane source strengths are not notably affected by requiring the agricultural source to scale exponentially with world population. The uncertainties about the median source strengths (variances) are reduced and the medians shift slightly (none change by more than 2 Tg/yr) (Figure 2). Setting the agricultural source to scale with world population increases the likelihood that any scenario chosen to explain the $\delta^{13}CH_4$, $\delta D(CH_4)$, and CH_4 concentration data involves a decrease in the natural$_{Mic}$ source (15% increase, 6% no change, 79% decrease, median change of -6 Tg/yr) (Table 4). The increase in the agricultural source comes at a time when the global climate system was transitioning from medieval times (which are often considered to have been warm and dry, identified with the Medieval Warm Period in Europe) to the interval often called the Little Ice Age (which is often considered to have been cooler and wetter). Also, world population growth accelerated during our study interval [*McEvedy and Jones*, 1978].

5.3. Model Results of the Sensitivity Runs

[38] As expected, isotopic ratios of atmospheric methane are more sensitive to isotopic changes in the larger sources, and are most sensitive to isotopic changes in the sink, as it affects all sources (Figure 3). For instance, a +0.001 change in the KIE_{13C} ($-1‰$ change in the ϵ_{13C} value) of the sink causes the median source strength of biomass burning to shift from 39 Tg/yr during TS1 in the primary run to 24 Tg/yr during TS1 in the sensitivity run. However, for

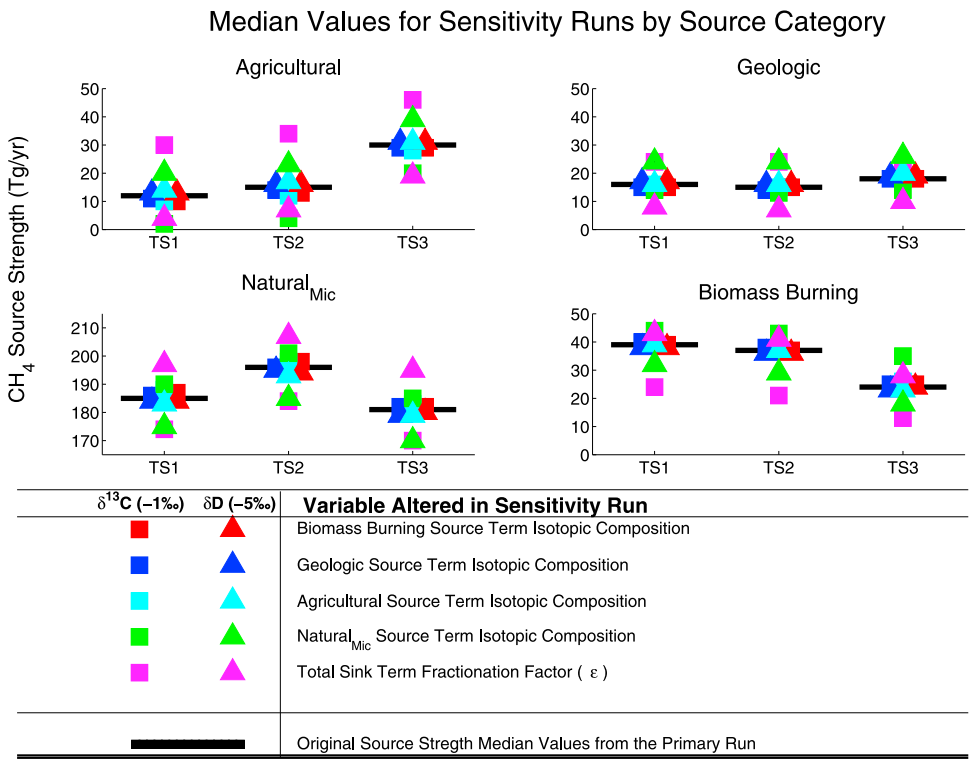

Figure 3. Sensitivity model run results for all source categories for TS1 (990–1460 CE), TS2 (1461–1575 CE) and TS3 (1589–1730 CE). Median emissions for each category from the primary run are denoted with horizontal lines. Results of the sensitivity runs are plotted with square and triangle symbols for $\delta^{13}CH_4$ and $\delta D(CH_4)$, respectively. Note that the perturbations applied in the sensitivity runs caused only small shifts in medians, and in no case changed the underlying time trend in median source strength.

the perturbations used here ($-1‰$ $\delta^{13}C$ and $-5‰$ δD), the differences between the estimated median source strengths in our sensitivity experiments and the corresponding medians in the primary run were not large, and the general time trends in median source strengths were unchanged (Figure 3), indicating robust temporal trends in the sources over our study interval.

6. Discussion

6.1. Primary Run Results: TS1 (990–1460 CE)

[39] The first time slice (TS1) is characterized by relatively low median agricultural emissions (12 Tg/yr), consistent with the relatively low population during this time. In the primary model run, median emissions from biomass burning (39 Tg/yr) are higher than estimates in most previous inventories [*Ferretti et al.*, 2005; *Lassey et al.*, 2007] but do agree with values found recently by *Fischer et al.* [2008] for numerous time intervals from the last glacial maximum to the present. As shown by the sensitivity runs, the magnitude of the biomass burning source median can be reduced (24 Tg/yr) to agree with *Ferretti et al.* [2005] by changing the KIE_{13C} of the cumulative methane sink by +0.001 ($-1‰$ change in the ϵ_{13C} value), but this adjustment then leaves a higher agricultural source median (30 Tg/yr) for the earlier time slice than expected by *Ruddiman and Thomson* [2001]. The median $natural_{Mic}$ emissions (185 Tg/yr) are very close to the preindustrial estimate used by *Lassey et al.* [2007], while the median contribution from natural gas venting/leakage is significantly lower than the value presented by *Etiope et al.* [2008], but much more similar to the value used by *Lassey et al.* [2007]. The geologic source is nearly constant across all three time slices, with its median never departing by more than 2 Tg/yr from 16 Tg/yr. The second time slice (TS2) is based on fewer points, though we find no basis for combining TS2 with TS1 or TS3. In order to focus on the maximum change in the isotopic records, we have chosen to forgo an in-depth discussion of TS2, but we include comparisons with the other time slices for completeness.

6.2. Primary Run Results: TS3 (1589–1730 CE)

[40] The median agricultural source increased by 60 ± 1% (18 Tg/yr) from TS1 to TS3 while the mean increase in world population was ~38 ± 6%. Almost 70% of all valid scenarios included an increase in the agricultural source that was larger than the corresponding increase in world population (38%). This larger-than-expected increase in agricultural methane may reflect improvements in technology allowing larger areas to be farmed, or a large-scale shift to rice cultivation as parts of Southeast Asia became wetter during the onset of the LIA [*Chen et al.*, 2005; *Wang et al.*, 2005; *Page et al.*, 2004; *Paulsen et al.*, 2003; *Chu et al.*, 2002; *Hong et al.*, 2001]. The median biomass burning

source strength decreased by 38 ± 1% (15 Tg/yr) from TS1 to TS3. Just prior to TS3 there is a sudden drop (~20 ppb on average) in CH_4 accompanied by a drop in both the $\delta D(CH_4)$ and $\delta^{13}CH_4$ (Figure 1). A sudden drop in the biomass burning source strength at this time is corroborated by *Marlon et al.* [2008], and suggested by *Ferretti et al.* [2005] to be due to the massive plagues that accompanied European contact in the Americas.

[41] Alternatively, *Houweling et al.* [2008] suggested that the Northern Hemisphere (NH) cooling of the LIA indicated by *Moberg et al.* [2005] was sufficient to explain much of the abrupt 20 ppb drop in CH_4 during the 1580s [see also *Etheridge et al.*, 1998; *MacFarling-Meure et al.*, 2006]. Decreased temperatures have a negative effect on CH_4 emission from wetlands, particulary high latitude wetlands [*Worthy et al.*, 2000]. However, the updated ensemble of *Mann et al.* [2008] shows the record [*Moberg et al.*, 2005] to have a much more pronounced NH temperature decrease during the MWP/LIA transition than most other records [see also *Jansen et al.*, 2007]. From *Mann et al.* [2008] we get a mean NH temperature change of −0.1°C and a maximum change of −0.6°C around the 1580s when the abrupt drop in methane concentrations took place [see also *Gerber et al.*, 2003]. To estimate the impact of this cooling, we follow [*Houweling et al.*, 2008]:

$$E_{CH_4} = E^0_{CH_4} * Q_{10}^{\alpha\left(T^1_{NH}-T^2_{NH}\right)/10} \quad (1)$$

A Q_{10} value of 7 (predicting a 7-fold decrease in methane emission with a 10°C decrease in temperature) is selected from the literature [*Worthy et al.*, 2000] and an α value (a scaling factor designed to take into account the difference between average NH temperature and the temperature of the methane-producing regions) of 1 is retained due to the lack of a robust alternative. $E_{CH_4}{}^0$ is the initial emission rate and E_{CH_4} is the perturbed emission rate taking into account some temperature change defined by T^1_{NH} and T^2_{NH}. According to this relationship, a temperature drop of 0.1°C would produce only a 2.8 ppb drop in atmospheric methane from a decrease in the global $natural_{Mic}$ emissions alone, while the maximum 0.6°C drop would result in a 16 ppb decrease. Thus, if a uniform temperature decrease and corresponding Q_{10} value is applied to the global $natural_{Mic}$ source, it appears that the maximum Little Ice Age cooling as indicated in the *Mann et al.* [2008] ensemble approaches the 20 ppb threshold needed to explain the CH_4 decrease in the 1580s CE. However, if the mean temperature change is assumed, additional decreases associated with the biomass burning source (as our model and the work of *Marlon et al.* [2008] suggest) could explain this CH_4 decrease.

7. Conclusions

[42] New ice-core data from the WAIS Divide site in central West Antarctica document changes in $\delta D(CH_4)$ and $\delta^{13}CH_4$ over the last 1000 years. There is remarkable agreement between our $\delta^{13}CH_4$ data and those of *Ferretti et al.* [2005] despite being produced in different laboratories on different ice cores, providing strong confidence that these data successfully record the atmospheric history. Our new $\delta D(CH_4)$ data exhibit time trends that correlate closely with $\delta^{13}CH_4$. Any hypotheses for the history of atmospheric methane sources and sinks over this important time interval can be tested against the history of atmospheric methane concentration and dual isotopic ratios, as presented here.

[43] Because of the diversity of methane sources, a unique inversion is not possible for the time history of those sources together with any changes in their isotopic compositions and in methane sinks. We have, however, conducted a simple box-modeling exercise to assess likely histories for the time interval from 990–1730 CE. We chose three time slices within this larger interval when methane concentrations were relatively stable. We then averaged each data set (CH_4 concentrations, $\delta D(CH_4)$, and $\delta^{13}CH_4$), over each time slice and attempted to match all three values in all three slices using a simple box model driven by varying strengths of sources assumed to have constant isotopic compositions together with constant sink fractionation. We find that an increasing agricultural source and a decreasing biomass-burning source, with most of the change between the 1500s and the 1600s, best fits our data, and that this result is relatively insensitive to the changes in source isotopic compositions or sink isotopic fractionation attempted in this study. The agricultural source scales closely with population, and changes in the biomass burning source may reflect changes in the Americas following European contact, or other processes.

[44] **Acknowledgments.** This material is based upon work supported under a National Science Foundation Graduate Research Fellowship. This work has been supported by NSF grants ANT 04-40759 and NSF OPP 0424589, 0520470, and 0539578 as well as support from the Gary Comer Science and Education Foundation. We would like to recognize Eric Cravens and the NICL staff for help with the processing and data management as well as ICDS for drilling. Also thanks to Denny Walizer and George Wood for analytical help and Isaac Gerg, Roman Tonkonojenkov, Ruth Hummel, and Brian LeVay for help with computer modeling and statistics.

References

Allan, W. H., H. Struthers, and D. Lowe (2007), Methane carbon isotope effects caused by atomic chlorine in the marine boundary layer: Global results compared with Southern Hemisphere measurements., *J. Geophys. Res.*, *112*, D04306, doi:10.1029/2006JD007369.

Andres, R. J., D. J. Fielding, G. Marland, T. A. Boden, N. Kumar, and A. T. Kearney (1999), Carbon dioxide emissions from fossil-fuel use, 1751–1950, *Tellus, Ser. B*, *51*, 759–765.

Battle, M., et al. (1996), Atmospheric gas concentrations over the past century measured in air from firn at the South Pole, *Nature*, *383*, 231–235.

Bergamaschi, P. (1997), Seasonal variations of stable hydrogen and carbon isotope ratios in methane from a Chinese rice paddy, *J. Geophys. Res.*, *102*, 25,383–25,393.

Chanton, J. P., G. J. Whiting, N. E. Balir, C. W. Lindau, and P. K. Bollich (1997), Methane emission from rice: Stable isotopes, diurnal variations, and CO_2 exchange, *Global Biogeochem. Cycles.*, *11*, 15–27.

Chen, J. C., G. Wan, D. D. Zhang, Z. Chen, J. Xu, T. Xiao, and R. Huang (2005), The "Little Ice Age" recorded by sediment chemistry in Lake Erhai, southwest China, *Holocene*, *15*, 925–931, doi:10.1191/0959683605hl863rr.

Chu, G., J. Liu, Q. Sun, H. Lu, Z. Gu, W. Wang, and T. Liu (2002), The "Medieval Warm Period" drought recorded in Lake Huguangyan, tropical South China, *Holocene*, *12*, 511–516, doi:10.1191/0959683602hl566ft.

Etheridge, D. M., L. P. Steele, R. J. Francey, and R. L. Langenfelds (1998), Atmospheric methane between 1000 A.D. and present: Evidence of anthropogenic emissions and climatic variability, *J. Geophys. Res.*, *103*, 15,979–15,993.

Etiope, G., L. K. R., R. W. Klusman, and E. Boschi (2008), Reappraisal of the fossil methane budget and related emission from geologic sources, *Geophys. Res. Lett.*, *35*, L09307, doi:10.1029/2008GL033623.

Ferretti, D. F., et al. (2005), Unexpected changes to the global methane budget over the past 2000 years, *Science*, *309*, 1714–1717.
Fischer, H., et al. (2008), Changing boreal methane sources and constant biomass burning during the last termination, *Nature*, *452*, 864–867.
Gerber, S., F. Joos, P. Brugger, T. F. Stocker, M. E. Mann, S. Sitch, and M. Scholze (2003), Constraining temperature variations over the last millennium by comparing simulated and observed atmospheric CO_2, *Clim. Dyn.*, *20*, 281–289.
Han, G. H., H. Yoshikoshi, H. Nagai, T. Yamada, M. Saito, A. Miyata, and Y. Harazonio (2005), Concentration and carbon isotope profiles of CH_4 in paddy rice canopy: Isotopic evidence for changes in CH_4 emission pathways upon drainage, *Chem. Geol.*, *218*, 25–40.
Hong, Y. T., et al. (2001), A 6000-year record of changes in drought and precipitation in northeastern China based on a $\delta^{13}C$ time series from peat cellulose, *Earth Planet. Sci. Lett.*, *185*, 111–119.
Houweling, S., F. Dentener, and J. Lelieveld (2000a), The modeling of tropospheric methane: How well can point measurements be reproduced by a global model?, *J. Geophys. Res.*, *105*, 8981–9002.
Houweling, S., F. Dentener, and J. Lelieveld (2000b), Simulation of preindustrial methane to constrain the global source strenght of natural wetlands, *J. Geophys. Res.*, *105*, 17,243–17,255.
Houweling, S., G. R. van der Werf, K. K. Goldewijk, T. Rockmann, and I. Aben (2008), Early anthropogenic CH_4 emissions and the variation of $\delta^{13}CH_4$ over the last millennium, *Global Biogeochem. Cycles*, *22*, GB1002, doi:10.1029/2007GB002961.
Jansen, E., et al. (2007), Palaeoclimate, in *Climate Change 2007. The Physical Science Basis. Contribution of Working Group 1 to the Fourth Assessment Report of the Intergovernmental Panel on Climate Change*, edited by S. Solomon et al., pp. 434–497, Cambridge Univ. Press, Cambridge, U. K.
Keppler, F., J. T. G. Hamilton, M. Brab, and T. Rockmann (2006), Methane emissions from terrestrial plants under aerobic conditions, *Nature*, *439*, 187–191.
Khalil, M. A. K. (Ed.) (1993), *Stable Isotopes in Global Budgets*, Springer, New York.
Knox, M., P. D. Quay, and D. Wilbur (1992), Kinetic isotopic fractionation during air-water gas ransfer of O_2, N_2, CH_4, and H_2, *J. Geophys. Res.*, *97*, 20,335–20,343.
Kruger, M., G. Eller, R. Conrad, and P. Frenzel (2002), Seasonal variation in pathways of CH_4 production and in CH_4 oxidation in rice fields determined by stable carbon isotopes and specific inhibitors, *Global Change Biol.*, *8*, 265–280.
Lassey, K. R., D. C. Lowe, and M. R. Manning (2000), The trend in atmospheric methane and $\delta^{13}C$ and implications for isotopic constraints on the global methane budget, *Global Biogeochem. Cycles*, *14*, 41–49.
Lassey, K. R., D. M. Etheridge, D. C. Lowe, A. M. Smith, and D. F. Ferretti (2007), Centennial evolution of the atmospheric methane budget: what do the carbon isotopes tell us?, *Atmos. Chem. Phys.*, *7*, 2119–2139.
Levin, I., P. Bergamaschi, H. Dorr, and D. Trapp (1993), Stable isotopic signature of methane from major sources in Germany, *Chemosphere*, *26*, 161–177.
MacFarling-Meure, C., D. Etheridge, C. Trudinger, P. Steele, R. Langenfelds, T. van Ommen, A. Smith, and J. Elkins (2006), Law dome CO_2, CH_4 and N_2O ice core records extended to 2000 years BP, *Geophys. Res. Lett.*, *33*, L14810, doi:10.1029/2006GL026152.
Mahieu, K., A. DeVisscher, P. A. Vanrolleghem, and O. VanCleemput (2006), Carbon and hydrogen isotope fractionation by microbial methane oxidation: Improved determination, *Waste Manage.*, *26*, 389–398.
Mann, M. E., Z. Zhang, M. K. Hughes, R. S. Bradley, S. K. Miller, and S. Rutherford (2008), Proxy-based reconstructions of hemispheric and global surface temperature variations over the past two millennia, *Proc. Natl. Acad. Sci. U. S. A.*, *105*, 13,252–13,257.
Marik, T. (1998), Atmospheric $\delta^{13}C$ and δD measurements to balance the global methane budget, Ph.D thesis, Max Plank Inst.
Marlon, J. R., P. J. Bartlein, C. Carcaillet, D. G. Gavin, S. P. Harrison, P. E. Higuera, F. Joos, M. J. Power, and I. C. Prentice (2008), Climate and human influences on global biomass burning over the past two millennia, *Nat. Geosci.*, *1*, 697–702.
McConnell, J. R., G. W. Lamorey, S. W. Lambert, and K. C. Taylor (2002), Continuous ice-core chemical analyses using inductively coupled plasma mass spectrometry, *Environ. Sci. Technol.*, *36*, 7–11.
McEvedy, C., and R. Jones (Eds.) (1978), *Atlas of World Population History*, 368 pp., Penguin, Harmondsworth, U. K.
Moberg, A., D. M. Sonechkin, K. Holmgren, N. M. Datsenko, and W. Karlen (2005), Highly variable Northern Hemisphere temperatures reconstructed from low- and high-resolution proxy data, *Nature*, *433*, 613–617.
Nakagawa, F., N. Yoshida, A. Sugimoto, E. Wada, T. Yoshioka, S. Ueda, and P. Vijarnsorn (2002), Stable isotope and radiocarbon compositions of methane emitted from tropical rice paddies and swamps in southern Thailand, *Biogeochemistry*, *61*, 1–19.
Ott, R. L., and M. Longnecker (Eds.) (2001), *An Introduction to Statistical Methods and Data Analysis*, 5th ed., 308–314 pp., Duxbury, Pacific Grove, Calif.
Page, S. E., R. A. J. Wust, D. Weiss, J. O. Rieley, W. Shotyk, and S. H. Limin (2004), A record of late pleistocene and holocene carbon accumulation and climate change from an equatorial peat bog (Kalimantan, Indonesia): implications for past, present, and future carbon dynamics, *J. Quat. Sci.*, *19*, 625–635.
Paulsen, D. E., H. C. Li, and T. L. Ku (2003), Climate variability in central China over the last 1270 years revealed by high-resolution stlagmite records, *Quat. Sci. Rev.*, *22*, 691–701.
Pongratz, J., C. Reick, T. Raddatz, and M. Claussen (2008), A reconstruction of global agricultural areas and land cover for the last millennium, *Global Biogeochem. Cycles*, *22*, GB3018, doi:10.1029/2007GB003153.
Quay, P., J. Stutsman, D. Wilbur, A. Snover, E. Dlugokencky, and T. Brown (1999), The isotopic compsition of atmospheric methane, *Global Biogeochem. Cycles*, *13*, 445–461.
Reeburgh, W. S. (2004), Global methane biogeochemistry, *Treat. Geochem.*, *4*, 65–89.
Rhee, T. S., C. A. M. B., M. Brab, and C. Bruhl (2006), Isotopic composition of H_2 from CH_4 oxidation in the stratosphere and the troposphere, *J. Geophys. Res.*, *111*, D23303, doi:10.1029/2005JD006760.
Rice, A., A. A. Gotoh, H. O. Aijie, and S. C. Tyler (2001), High-precision continuous-flow measurements of $\delta^{13}C$ and δD of atmospheric CH_4, *Anal. Chem.*, *73*, 4104–4110.
Rice, A. L., S. C. Tyler, M. C. McCarthy, K. A. Boering, and E. Atlas (2003), Carbon and hydrogen isotopic compositions of stratospheric methane: 1. high-precision observations from the NASA ER-2 aircraft, *J. Geophys. Res.*, *108*(D15), 4460, doi:10.1029/2002JD003042.
Ruddiman, W. F., and J. S. Thomson (2001), The case for human causes of increased atmospheric CH_4, *Quat. Sci. Rev.*, *20*, 1769–1777.
Rust, F. (1981), Ruminant methane ($\delta^{13}C/\delta D$) values: Relation to atmospheric methane, *Science*, *211*, 1044–1046.
Saueressig, G., J. N. Crowley, P. B. nad C. Bruhl, C. A. M. Brenninkmeijer, and H. Fischer (2001), Carbon 13 and D kinetic isotope effects in the reactions of CH_4 with O(D) and OH: New laboratory measurements and their implications for the isotopic composition of stratospheric methane, *J. Geophys. Res.*, *106*, 23,127–23,138.
Sessions, A. L., T. W. Burgoyne, and J. M. Hayes (2001), Determination of the H_3 factor in hydrogen isotope ratio monitoring mass spectrometry, *Anal. Chem.*, *73*, 200–207.
Sowers, T. (2006), Late Quaternary atmospheric CH_4 isotope record suggests marine clathrates are stable, *Science*, *311*, 838–840.
Sowers, T. (2009), Atmospheric methane isotope records covering the holocene period, *Quat. Sci. Rev.*, doi:10.1016/j.quascirev.2009.05.023, in press.
Sowers, T. A., M. L. Bender, and D. Raynaud (1989), Elemental and isotopic composition of occluded O_2 and N_2 in polar ice, *J. Geophys. Res.*, *94*, 5137–5150.
Sowers, T., S. Bernard, O. Aballain, J. Chappellaz, J. M. Barnola, and T. Marik (2005), Records of the $\delta^{13}C$ of atmospheric CH_4 over the last 2 centuries as recorded in Antarctic snow and ice, *Global Biogeochem. Cycles*, *19*, GB2002, doi:10.1029/2004GB002408.
Tans, P. P. (1997), A note on isotopic ratios and the global atmospheric methane budget, *Global Biogeochem. Cycles*, *11*, 77–81.
Trudinger, C. M., I. G. Enting, D. M. Etheridge, R. J. Francey, V. A. Levchenko, and L. P. Steele (1997), Modeling air movement and bubble trapping in firn, *J. Geophys. Res.*, *102*, 6747–6763.
Turner, M. E., J. V. Beckett, and B. Afton (Eds.) (2001), *Farm Production in England, 1700–1914*, 133–172 pp., Oxford Univ. Press, Oxford, U. K.
Tyler, S. C., G. W. Brailsford, K. Yagi, K. Minami, and R. J. Cicerone (1994), Seasonal variations in methane flux and $\delta^{13}CH_4$ values for rice paddies in Japan and their implications, *Global Biogeochem. Cycles*, *8*, 1–12.
Tyler, S. C., A. L. Rice, and H. O. Ajie (2007), Stable isotope ratios in atmospheric CH_4: Implications for seasonal sources and sinks, *J. Geophys. Res.*, *112*, D03303, doi:10.1029/2006JD007231.
Uzaki, M., H. Mizutani, and E. Wada (1991), Carbon isotope composition of CH_4 from rice paddies in Japan, *Biogeochemistry*, *13*, 159–175.
Wang, Y., et al. (2005), The Holocene asian monsoons: Links to solar changes and North Atlantic climate, *Science*, *308*, doi:10.1126/science.1106,296.

Worthy, D. E. J., I. Levin, F. Hopper, M. K. Ernst, and N. B. A. Trivett (2000), Evidence for a link between climate and northern wetland methane emissions, *J. Geophys. Res.*, *105*, 4031–4038.

Wuebbles, D. J., and K. Hayhoe (2002), Atmospheric methane and global change, *Earth Sci. Rev.*, *57*, 177–210.

Yamada, K., Y. Ozaki, F. Nakagawa, S. Sudo, and H. Tsuruta (2006), Hydrogen and carbon isotopic measurements of methane from agricultural combustion: Implications for isotopic signatures of global biomass burning sources, *J. Geophys. Res.*, *111*, D16306, doi:10.1029/2005JD006750.

R. B. Alley, J. A. Mischler, and T. A. Sowers, Department of Geosciences, Pennsylvania State University, Deike Building 213, University Park, PA 16802, USA. (ralley@essc.psu.edu; john.mischler@gmail.com; sowers@geosc.psu.edu)

M. Battle, Department of Physics and Astronomy, Bowdoin College, 8800 College Station, Brunswick, ME 04011-8488, USA. (mbattle@bowdoin.edu)

J. R. McConnell, Hydrologic Sciences Division, Desert Research Institute, 2215 Raggio Pkwy., Reno, NV 89512, USA. (joe.mcconnell@dri.edu)

L. Mitchell, Department of Geosciences, Oregon State University, Corvallis, OR 97331, USA. (mitchelo@geo.oregonstate.edu)

T. Popp, Centre for Ice and Climate, Niels Bohr Institute, University of Copenhagen, Juliane Maries Vej 30 DK-2100 Copenhagen, Denmark. (trevor@gfy.ku.dk)

E. Sofen, Department of Atmospheric Sciences, University of Washington, 408 ATG Bldg., Box 351640, Seattle, WA 98195-1640, USA. (esofen@atmos.washington.edu)

M. K. Spencer, Department of Geology and Physics, Lake Superior State University, Sault Ste. Marie, MI 49783, USA. (mspencer@lssu.edu)